Evaluating the Effectiveness of Wenner Mode Configurations for Resistivity-based Moisture Monitoring in Compressed Earth Bricks

Tuan Anh Nguyen
STASD Research Group, Ho Chi Minh City University of Transport, Ho Chi Minh City, Vietnam
tuananh.nguyen@ut.edu.vn (corresponding author)

Minh Dung Pham
Vietnam Institute of Architecture, Vietnam
phamminhdung@muce.edu.vn

Nicolas Angellier
Civil Engineering Laboratory, Diagnostic and Sustainability (GC2D), University of Limoges, France
nicolas.angellier@unilim.fr

Laurent Ulmet
Civil Engineering Laboratory, Diagnostic and Sustainability (GC2D), University of Limoges, France
laurent.ulmet@unilim.fr

Frederic Dubois
Civil Engineering Laboratory, Diagnostic and Sustainability (GC2D), University of Limoges, France
frederic.dubois@unilim.fr

Received: 7 August 2024 | Revised: 31 August 2024 | Accepted: 4 September 2024

 DOI: https://doi.org/10.48084/etasr.8649

ABSTRACT

Compressed Earth Bricks (CEBs) have emerged as an eco-friendly construction material, although their properties are highly moisture dependent. This study investigated the applicability of electrical resistivity techniques for non-destructive moisture assessment in CEBs and determined the optimal electrode configurations for small-scale CEB samples. Various Wenner array electrode configurations, including Wenner Alpha, Beta, and Gamma arrangements, were tested on CEB specimens across a wide range of relative humidity levels. Numerical modeling using the finite element method was employed to simulate the current diffusion process in CEB samples. A mathematical formulation was developed to calculate the true electrical resistivity of the specimens based on the measured resistance and the geometric factors obtained from the numerical model. The results show that the electrical resistivity of CEBs exhibited a logarithmic relationship with moisture content, and the Wenner Alpha and Gamma configurations were proved to be the most suitable for small-scale samples. The proposed approach demonstrates the feasibility of continuous non-destructive moisture monitoring of CEBs to improve quality control.

Keywords-compressed earth bricks; moisture monitoring; electrical resistivity measurements; hygroscopic material

I. INTRODUCTION

Electrical resistivity techniques have emerged as a powerful non-destructive testing and characterization tool in various fields, particularly in geotechnical engineering [1-4]. These methods have been extensively researched, developed, and applied over the past several decades, gaining recognition for their versatility, reliability, and non-destructive nature.

Compressed Earth Bricks (CEBs) have gained increasing attention as a sustainable and eco-friendly alternative to conventional building materials [5-7]. CEBs offer numerous advantages, such as low embodied energy, natural biodegradability, and efficient production methods [8, 9]. However, similar to many earth-based materials, CEBs are highly hygroscopic [10, 11], meaning that their properties are significantly influenced by the moisture content [12-14].

Moisture content plays a crucial role in determining the strength, durability, and dimensional stability of CEBs [15]. An accurate assessment of moisture content is essential for quality control during the production and performance monitoring of CEB structures. In this context, electrical resistivity techniques have emerged as promising tools for non-destructive moisture assessment in various materials, including soils [16-18], steel [19], and concrete [20-22]. Notably, previous studies have demonstrated the effectiveness of electrical resistivity methods in assessing the moisture content of wood samples [23-25], a hygroscopic material with high electrical resistivity. This suggests the potential applicability of these techniques in CEBs. Electrical resistivity methods rely on the principle that the electrical resistivity of a material is sensitive to changes in its moisture content, and water being a good conductor of electricity. However, given the finite size of materials like wood and CEB samples, employing electrode configurations with large spacings, as commonly used in geotechnical applications, may pose challenges due to the limited sample dimensions. Therefore, this study focuses on investigating suitable electrode configurations for finite-sized samples.

Given the proven effectiveness of electrical resistivity techniques in geotechnical engineering and their potential for non-destructive moisture assessment in CEBs, this study aims to bridge the gap between these two domains. The main objective was to investigate the applicability of electrical resistivity methods for measuring the moisture content in CEBs and to develop reliable interpretation models for quantifying the resistivity of homogeneous CEB samples. First, the fundamental principles of the electrical resistivity method and the different electrode configurations used in this study are presented. Next, the experimental protocol for sample preparation and the hydric and electrical resistivity measurements are described in detail. Subsequently, the numerical approach based on finite element modeling to simulate the current diffusion process in the CEB sample is explained. Finally, the experimental and numerical results are presented and discussed, highlighting the optimal electrode configuration for CEB moisture assessment and the limitations of the method at low moisture content.

II. THEORY OF THE ELECTRICAL RESISTIVITY METHOD

A. Fundamental Principles

Electrical resistivity methods are based on the principle of measuring the resulting potential difference of an applied electric current in a material or medium. The resistivity of a material, an intrinsic property that quantifies its ability to resist the flow of electric current, is defined as the resistance per unit volume of the material and is expressed in ohm-meters (Ωm).

In a homogeneous and isotropic medium, the resistivity (ρ) is related to the measured resistance (R) by the following equation:

$$\rho = R\frac{A}{L} \quad (1)$$

where A is the cross-sectional area perpendicular to the current flow and L is the length of the material through which the current flows.

In practical applications, the procedure for assessing subsurface resistivity involves sequentially arranging four electrodes on the surface. A precisely measured direct current or low-frequency alternating current is applied between electrodes A and B, while the potential difference is measured between electrodes M and N, referred to as potential electrodes.

The apparent resistivity can be calculated using the following formula:

$$\rho_{app} = K\frac{\Delta V_{MN}}{I_{AB}} \quad (2)$$

where K is a geometric factor that depends on the arrangement and spacing of electrodes.

The geometric factor is expressed as:

$$K = \frac{2\pi}{\left(\frac{1}{AM}-\frac{1}{BM}\right)-\left(\frac{1}{AN}-\frac{1}{BN}\right)} \quad (3)$$

B. Electrode Configurations

The selection of an appropriate electrode array configuration is crucial for obtaining high-quality data from electrical resistivity surveys. Various electrode configurations have been developed, each with its own advantages and limitations concerning the depth of investigation, sensitivity to vertical and horizontal variations in subsurface resistivity, horizontal data coverage, and signal strength [17, 24].

This study focuses on analyzing the effectiveness of resistivity measurements using a Wenner array. Specifically, in the study were examined three Wenner array configurations (Wenner Alpha, Beta, and Gamma) for subsurface resistivity experiments.

In geophysical applications, the Wenner Alpha array, also known as the "normal" Wenner array, excels at detecting vertical variations in subsurface resistivity, particularly directly beneath the center of the array. The Wenner Beta array, a modification of the dipole-dipole array with uniform electrode spacing, provides an alternative method. It is particularly sensitive to subsurface features and excels in identifying high resistivity anomalies near the edges of the array, offering a more refined perspective on lateral variations than the Wenner Alpha configuration. The Wenner Gamma array, a variant of the Wenner-Schlumberger array with evenly spaced electrodes, demonstrates a unique sensitivity profile owing to its distinctive interleaved current and potential electrode setup. The deepest regions of the maps are located below the two outer electrodes, marking a departure from the central emphasis observed in the Alpha and Beta configurations. By investigating these three Wenner configurations, this study aimed to determine the optimal arrangement for assessing the specific material under investigation and develop reliable interpretation models for quantifying the resistivity of homogeneous samples.

III. EXPERIMENTAL PROTOCOL

A. Sample Preparation

The bricks used in this study were sourced from a brick manufacturing plant in the southwest region of France, where they were produced through vacuum extrusion. The vacuum extrusion process introduces a degree of anisotropy in the bricks due to the orientation of the clay slabs, resulting in variations in the hydric, thermal, and mechanical properties of the bricks in two directions: perpendicular and parallel to the extrusion direction [26]. The bricks had dimensions of 225 x 110 x 50 mm^3. For this study, smaller specimen samples measuring 50 × 40 × 40 mm^3 were cut from the original full bricks. This size reduction was intended to shorten the duration of the hydric experiments and facilitate the electrical resistivity measurements.

B. Hydric Experiments

The electrical resistivity measurements were conducted on the brick samples under varying relative humidity conditions to investigate the influence of moisture content on the resistivity of the material. A desiccator-based humidity control system was employed to subject the samples to a wide range of stable relative humidity levels.

The desiccator apparatus allows for precise regulation of the ambient environment by establishing defined relative humidity conditions, which are determined by the quantities of water and salt present. The desiccant salt absorbs or releases moisture until equilibrium relative humidity is reached, ensuring stable humidity conditions within the desiccator over time.

The brick samples were placed inside the desiccator and exposed to six progressively lower target Relative Humidity (RH) setpoints: 100%, 70%, 60%, 50%, 40%, and 20%. At each setpoint, the samples were allowed to equilibrate until they reached a stable moisture content, which corresponded directly to the equilibrated RH level. The equilibration process ensured that the moisture distribution within the samples was uniform and representative of specific humidity conditions.

The desiccator-based environmental control method provides a controlled and stable method for evaluating the influence of the moisture content on the resistivity of the sample. By covering a wide range of RH levels, from saturation (100% RH) to dry conditions (20% RH), the experimental procedure enabled a comprehensive characterization of the resistivity-moisture relationship. To quantify the moisture content of the brick samples at each relative humidity setpoint, gravimetric measurements were conducted. The samples were weighed after reaching equilibrium at each humidity level and compared to their dry mass, which was obtained by drying the samples in an oven at a suitable temperature until no further change in mass was observed. The moisture content (w) was calculated as the ratio of the mass of water to the dry mass (m_0) of the sample, expressed as a percentage:

$$w = \frac{m-m_0}{m_0}(\%) \quad (4)$$

where m is the mass of the sample at a given moisture content.

The hydric experiments demonstrated that the saturation moisture content of the CEB sample varied according to an exponential function of the relative humidity, as illustrated in Figure 1. This behavior is characteristic of the hygroscopic properties of porous materials, such as CEBs. Notably, across the relative humidity range of 20-100%, the moisture content of the tested sample fluctuated between 1.86% and 9.48%. This implies that even under saturated ambient humidity conditions, the moisture content of the CEB sample reached a threshold below 10%.

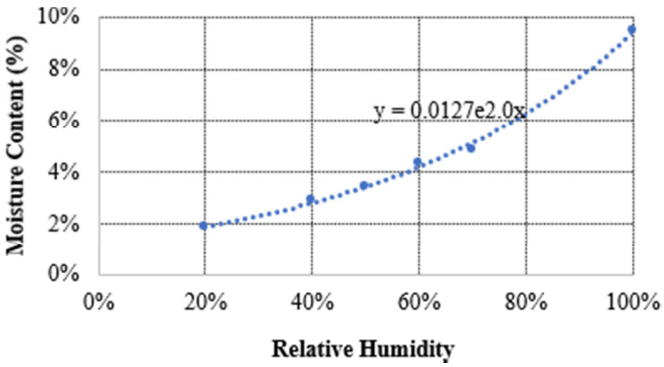

Fig. 1. Moisture content of CEB samples as a function of relative humidity.

C. Electrical Resistivity Experimental

Electrical resistivity measurements were conducted using a Syscal Junior resistivity meter (Figure 2), which is a device commonly used in geological surveys. The Syscal Junior is capable of performing electrical resistivity measurements in a standard four-electrode configuration consisting of two current electrodes that inject a direct current into the material and two potential electrodes that measure the resulting voltage drop. The Syscal Junior resistivity meter used in this study offers two measurement modes with different current injection levels: 1250 mA and 50 mA. These two modes were employed to measure the electrical resistivity of the CEBs samples, and the results obtained from both modes were compared and cross-validated to ensure measurement accuracy. The 1250 mA mode is the standard measurement mode of the Syscal Junior system, providing a higher current injection level suitable for a wide range of materials. On the other hand, the 50 mA mode, which is achieved through the integration of a current divider module, allows for more precise measurements by reducing the maximum injectable current. By utilizing both the 1250 mA and 50 mA modes, we aimed to obtain a comprehensive set of resistivity data for the CEB samples. The comparison and cross-validation of the results from these two modes help to ensure the reliability and robustness of the measurements, thereby enhancing the overall quality of the resistivity assessment.

One of the challenges encountered when measuring resistive samples, such as CEBs, is the accurate measurement of low current levels. While the resistivity of CEBs is not exceptionally high compared to that of other building materials, precise quantification of the currents passing through the samples remains important for accurate resistivity

determination. To address this requirement and enhance the sensitivity of the resistivity meter, a current divider module was integrated into the Syscal Junior system. The current divider module effectively reduced the maximum injectable current from 1250 mA to 50 mA, allowing for improved resolution in measuring the currents traversing the samples. The incorporation of the current divider module is advantageous for the analysis of small-scale compressed earth brick samples, as it enables the Syscal Junior system to accurately measure the current levels passing through the specimens, thereby improving the overall sensitivity and precision of the resistivity measurements. Since the brick test samples were small, on the scale of a few centimeters, specialized electrodes and cabling were required as opposed to conventional geophysical resistivity equipment designed for semi-infinite subsurface profiling. Figure 3 provides details on the custom electrode fabrication and connectivity for suitability to small brick specimens and precision resistivity quantification.

Fig. 2. Syscal Junior resistivity meter.

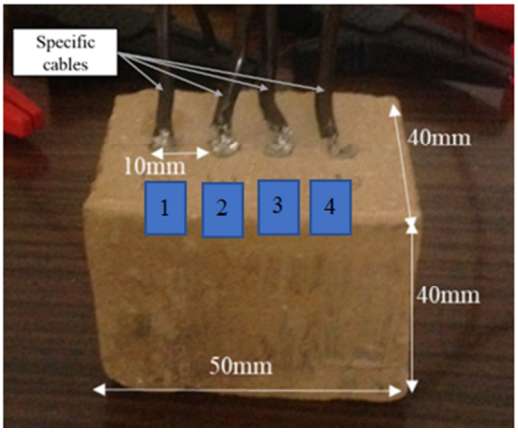

Fig. 3. CEB sample with specific cables and electrodes.

The electrodes used in the electrical resistivity measurements were fabricated by melting a tin-copper alloy and pouring it into cylindrical molds. This process allowed for the creation of durable and conductive electrodes with a shape that easily fits into the designated sensor insertion points in the compressed earth brick samples. The molded electrodes were then fitted with electrical cables to facilitate their connection to the resistivity measurement system.

To investigate the optimal electrode configuration for measuring the electrical resistivity of CEBs, 24 quadrupole configurations were considered, as presented in Table I. These configurations were based on the Wenner electrode system, which consists of four equally spaced electrodes arranged in a linear fashion. The 24 configurations are grouped into three distinct types: Wenner Alpha, Wenner Beta, and Wenner Gamma, each representing a specific arrangement of the current (A, B) and potential (M, N) electrodes.

In the Wenner Alpha configuration, the current electrodes occupy the outer positions (1 and 4), whereas the potential electrodes are placed in the inner positions (2 and 3). Eight different permutations were considered in this arrangement. The Wenner Beta configuration involves the current electrodes being adjacent to each other (1 and 2, or 3 and 4), with the potential electrodes occupying the remaining positions, resulting in eight variations. Lastly, the Wenner Gamma configuration features an alternating pattern of current and potential electrodes, with the current electrodes at positions 1 and 3 (or 2 and 4) and the potential electrodes in the remaining positions, yielding eight arrangements.

TABLE I. QUADRUPOLE CONFIGURATION

Mode		Configuration (A, B, M, N)
Wenner Alpha	A M N B	(1, 4, 2, 3), (1, 4, 3, 2), (2, 3, 1, 4), (2, 3, 4, 1),(3, 2, 1, 4), (3, 2, 4, 1), (4, 1, 2, 3), (4, 1, 3, 2)
Wenner Beta	A B M N	(1, 2, 3, 4), (1, 2, 4, 3), (2, 1, 3, 4), (2, 1, 4, 3),(3, 4, 1, 2), (3, 4, 2, 1), (4, 3, 1, 2), (4, 3, 2, 1)
Wenner Gamma	A M B N	(1, 3, 2, 4), (1, 3, 4, 2), (2, 4, 1, 3), (2, 4, 3, 1),(3, 1, 2, 4), (3, 1, 4, 2), (4, 2, 1, 3), (4, 2, 3, 1)

The electrical resistivity experiments were performed under two injection conditions for each quadrupole configuration, using both 1250 mA and 50 mA currents. The use of redundant datasets with different current levels provides internal validation and allows the assessment of potential current-dependent effects. By considering a comprehensive set of 24 electrode configurations and duplicating measurements at two current levels, this study obtained extensive resistivity data spanning moisture levels from saturated to completely desiccated states.

IV. NUMERICAL APPROACH

The generalized Ohm's and Fourier's laws demonstrate a clear analogy between electrical conduction and steady-state heat transfer [27]. Exploiting this relationship, the current diffusion process was modeled by implementing the Cast3M finite element code's heat transfer tools [28]. The model reflects the real sample and electrode dimensions for all configurations (Figures 4 and 5).

For parallelepiped specimens containing internal electrode arrays, generating a mesh encompassing the entire sample and electrode assembly is generally advised. However, the problem presented in this research possesses complete symmetry.

Consequently, rather than modeling the entire sample and its internal electrode system, it is sufficient to consider only half of the sample, as depicted in Figure 4. This approach significantly reduces computational complexity while maintaining an accurate representation of the current flow process through the sample between the electrode pairs. The electrodes were numbered sequentially from one to four, corresponding to their arrangement in the experimental setup.

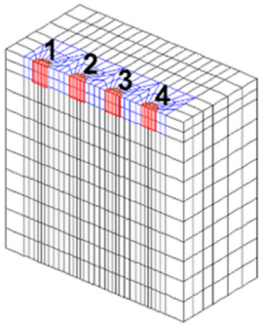

Fig. 4. Sample discretization.

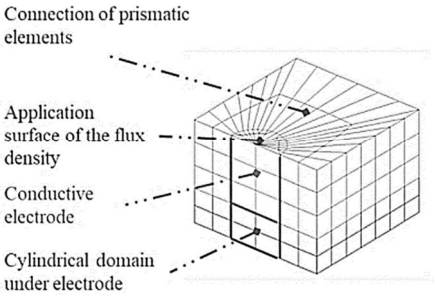

Fig. 5. Electrode modeling.

The electrodes were modeled in the form of cylinders connected to the specimen using prismatic elements (Figure 5). The current was applied at the top surface of the electrodes, which were modeled as perfectly conductive elements. In the experimental setup, the Syscal resistivity meter automatically adjusted the generated current intensity to ensure that the desired potential difference between the measuring electrodes was established. However, for the numerical model, due to the linear Ohm's law, the simulated resistance value remains independent of the applied potential or injected current. Therefore, the numerical model adopted a normalized injection current of 1 A for simplicity and consistency in the computational analysis.

In this case, for the numerical model, given any resistivity field of the sample, irrespective of the electrode positions, the configurations within each quadrupole group (Wenner Alpha, Beta, Gamma) yielded an identical value of the numerical difference potential. However, it should be noted that in real-world experimental settings, there might be inherent uncertainties or discrepancies between repeated measurements. In the context of a sample possessing a unit resistivity value, the numerical model facilitates the calculation of the corresponding resistance values, represented as $\left(\frac{\Delta V_{MN}}{I_{AB}}\right)_{num}$

According to the numerical values of $\Delta V_{MN}/I_{AB}$ presented in Table II for the Wenner configurations, significant differences are observed among the quadrupole groups. These disparities arise from the distinct geometrical factors associated with each configuration. The Wenner Beta configuration yielded the lowest $\Delta V_{MN}/I_{AB}$ value, indicating a higher sensitivity to the sample's resistivity. This is attributed to the closer spacing of the potential electrodes, resulting in a smaller measured potential difference $\Delta V_{MN}/I_{AB}$ for a given injection current. Conversely, the Wenner Alpha and Gamma configurations exhibit higher and similar $\Delta V_{MN}/I_{AB}$ numeric values. This similarity stems from the comparable electrode spacings and alternating arrangement of current and potential electrodes in both configurations. The higher values suggest a lower sensitivity to the sample's resistivity compared to the Wenner Beta configuration.

TABLE II. $\left(\frac{\Delta V_{MN}}{I_{AB}}\right)_{num}$ OF 3 TYPES OF QUADRUPOLES

Configuration mode	$\left(\frac{\Delta V_{MN}}{I_{AB}}\right)_{num}$ (Ω)
Wenner Alpha	16.42
Wenner Beta	3.11
Wenner Gamma	13.31

The differences in $\Delta V_{MN}/I_{AB}$ numeric values among the Wenner configurations highlight the importance of considering the electrode arrangement when interpreting resistivity measurements. The choice of configuration should account for factors such as the desired sensitivity, spatial resolution, and the expected resistivity distribution within the sample. Understanding the influence of electrode geometry on the measured resistivity response is crucial for accurate data interpretation and optimizing experimental designs for specific applications.

V. RESULTS AND DISCUSSION

Through a comparison of the resistance measurements on the sample obtained using two experimental modes, specifically 1250 mA and 50 mA, Figure 6 visually illustrates the observed deviation. It is noteworthy that the 1250 mA measurement mode is unable to measure resistance at relative humidity of 40% RH and 20% RH. The graphical representation demonstrates that as humidity decreases, the deviation between resistance measurements obtained from the two modes progressively increases. Importantly, beyond a humidity level of 50% RH, the average deviation between measurement modes became significantly pronounced. This suggests that, at least from a humidity level of 50% RH onwards, the resistance measurements obtained from the 1250 mA mode noticeably diverge from those acquired from the 50 mA mode, ultimately reaching a point where they could not be quantified.

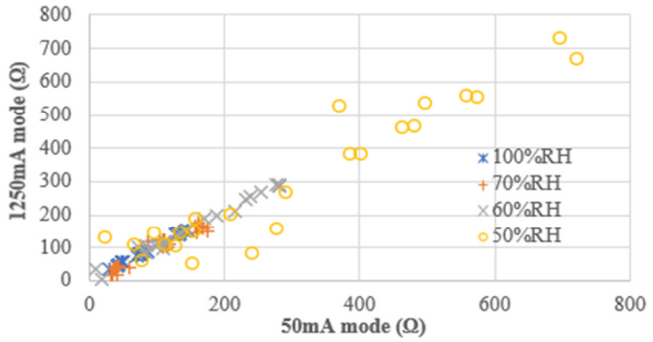

Fig. 6. The observed deviation of $\frac{\Delta V_{MN}}{I_{AB}}$ measured in the 50 mA and 1250 mA modes.

By comparing the two resistance measurement modes, it was observed that the 50 mA mode was able to obtain higher resistance values corresponding to the resistivity of the sample. This indicates that the 50 mA mode is more suitable for utilizing the measurement results in subsequent analysis. Therefore, when considering the standard sample, the measurement data obtained from the 50 mA mode were used for analysis purposes.

The standard deviation of the measured $\frac{\Delta V_{MN}}{I_{AB}}$ values, a measure of the dispersion of data around the mean, reveals that among the three Wenner array modes obtained from the 50 mA mode (Figure 7), Wenner Beta exhibits the highest deviation, corresponding to the greatest dispersion of measurement values relative to the other modes. Notably, Wenner Beta is essentially a Dipole-Dipole array with uniform electrode spacing. This indicates that while the Dipole-Dipole configuration proves effective in geotechnical applications (semi-infinite environments), it may not be suitable for smaller-sized samples. The other two measurement modes, Wenner Alpha and Gamma, show less dispersion in their results, with Wenner Alpha presenting the least variation.

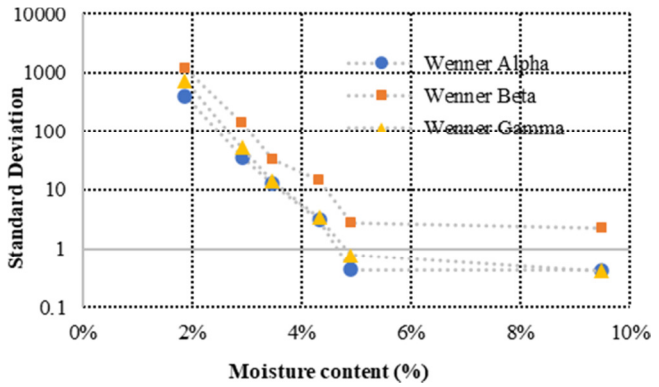

Fig. 7. Standard deviation of 3 configuration modes.

Figure 7 illustrates that as the moisture content of the CEB samples decreased, the standard deviations of the resistivity measurements across all three configurations became increasingly significant. This trend indicates that the reliability of the measured data decreased with lower moisture levels. To address this issue and extend the applicability of the electrical resistivity method to lower moisture content, future investigations could explore the use of equipment with higher measurement capacities or consider alternative electrode configurations that may improve the accuracy and precision of the measurements in the low-moisture range. Unlike electrical conduction in a semi-infinite medium, wherein (2) applies, the quantification of the geometric factor K_m for a finite volume necessitates modifications to account for the sample boundaries. In this confined transmission medium geometry, K_m exhibits dependence on both electrode configurations as well as specimen shape, deviating from the standard expressions:

$$\rho_{app} = K_m \frac{\Delta V_{MN}}{I_{AB}} \quad (5)$$

Considering a specimen of identical dimensions and electrode configurations to the experimental setup, possessing a homogeneous resistivity of unity, the numerical model facilitates computing the geometric factor K_m corresponding to the experimental arrangement. Thereby, the actual electrical resistivity ρ_{exp} can be quantified through the subsequent relationship:

$$\rho \frac{\left(\frac{\Delta V_{MN}}{I_{AB}}\right)_{exp}}{\left(\frac{\Delta V_{MN}}{I_{AB}}\right)^{1}_{num_{exp}}} \quad (6)$$

$\left(\frac{\Delta V_{MN}}{I_{AB}}\right)_{exp}$: $\frac{\Delta V_{MN}}{I_{AB}}$ measured.

According to (5), based on the measurement data obtained using the 50 mA mode and Wenner Alpha configuration, and the numerical models for the case of a homogeneous sample, the true electrical resistivity can be determined, as shown in Figure 8. It is evident that the electrical resistivity of the CEB sample exhibits a logarithmic relationship with moisture content. As the moisture content of the sample increases, the resistivity decreases exponentially, spanning the investigated range from 2% to 10% moisture content. However, it is important to note that the reliability of the measured data decreased as the moisture content of the CEB samples decreased.

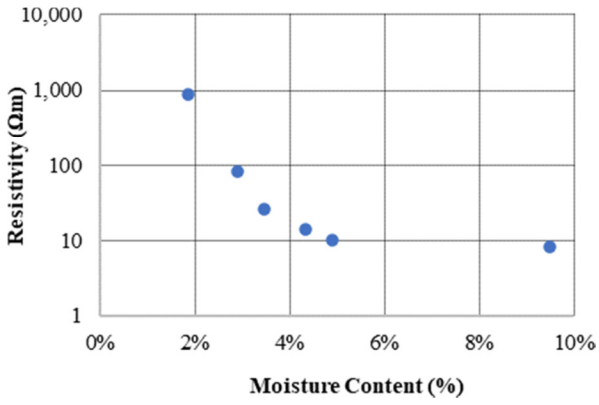

Fig. 8. Calculated resistivity of CEB sample.

This study demonstrated the feasibility of the electrical method in determining the electrical resistivity of CEB samples, but it also highlighted the challenges associated with measurements at lower moisture levels. The decreasing reliability of the data with lower moisture content suggests that additional experiments and methodological improvements are required to extend the applicability of this method to a wider range of moisture levels. Possible solutions include using instruments with higher measurement sensitivity or investigating alternative electrode configurations that may enhance the accuracy and precision of the measurements in the low moisture range.

VI. CONCLUSIONS

This study successfully demonstrated the feasibility and potential of applying electrical resistivity measurement techniques for non-destructive moisture assessment in CEBs. By integrating experimental resistivity measurements on CEB samples under varying moisture conditions with numerical modeling using the finite element method, this research provides a comprehensive investigation into the relationship between resistivity and moisture content in CEBs.We show the reliability of the resistivity technique for nondestructive moisture assessment in CEBs. Moreover, the Wenner Alpha and Gamma configurations were identified as more suitable for small-scale CEB samples compared to the Wenner Beta configuration, with the Wenner Alpha configuration exhibiting the most stable and consistent results.

A logarithmic relationship was observed between the resistivity and moisture content of CEBs, with resistivity decreasing exponentially as the moisture content increased from 2% to 10%. However, we recognized the decreased reliability of measurement data at low moisture content, as evidenced by high standard deviations.

The novelty of this work lies in its comprehensive approach to adapting electrical resistivity techniques for the specific context of small-scale compressed earth bricks. This study is one of the first to utilize electrical methods for moisture determination in CEBs, representing a significant advancement in the nondestructive testing of these sustainable building materials. Furthermore, this research uniquely combines detailed experimental measurements using various Wenner array configurations with finite element modeling to determine the true resistivity of CEBs across a range of moisture content.

The significance of this study is two-fold. It provides a methodology for nondestructive moisture assessment in CEBs, addressing the critical need for sustainable construction practices, and these findings pave the way for developing real-time moisture monitoring systems for earthen structures, potentially revolutionizing the quality control and maintenance practices in this field.

This study bridges the gap between geotechnical resistivity methods and sustainable construction materials, opening new avenues for research and applications in sustainable building technologies. Despite these promising results, limitations exist, particularly for moisture levels below 2%. Future research should focus on enhancing the measurement accuracy at low moisture levels and integrating electrical resistivity sensors into the CEB components for real-time monitoring.

In conclusion, this study demonstrates the significant potential of electrical resistivity techniques for sustainable construction using CEBs. This advances our understanding of moisture behavior in CEBs and lays the foundation for innovative monitoring systems to enhance the durability and performance of earthen structures. As the construction industry seeks sustainable alternatives, this research provides valuable tools for ensuring the quality and longevity of earth-based building materials.

ACKNOWLEDGMENTS

The authors gratefully acknowledge the support provided under project code KHTD2313/HD-DHGTVT from Ho Chi Minh City University of Transport (UTH).

REFERENCES

[1] A. P. Aizebeokhai, A. A. Oni, K. D. Oyeyemi, and O. Ogungbade, "Electrical resistivity imaging (ERI) data for characterising crystalline basement structures in Abeokuta, southwestern Nigeria," *Data in Brief*, vol. 19, pp. 2393–2397, Aug. 2018, https://doi.org/10.1016/j.dib.2018.07.034.

[2] J. D. Ducut *et al.*, "A Review of Electrical Resistivity Tomography Applications in Underground Imaging and Object Detection," *Displays*, vol. 73, Jul. 2022, Art. no. 102208, https://doi.org/10.1016/j.displa.2022.102208.

[3] I. Muchingami, D. J. Hlatywayo, J. M. Nel, and C. Chuma, "Electrical resistivity survey for groundwater investigations and shallow subsurface evaluation of the basaltic-greenstone formation of the urban Bulawayo aquifer," *Physics and Chemistry of the Earth, Parts A/B/C*, vol. 50–52, pp. 44–51, Jan. 2012, https://doi.org/10.1016/j.pce.2012.08.014.

[4] V. Vivaldi, P. Torrese, M. Bordoni, F. Viglietti, and C. Meisina, "ERT-based experimental integrated approach for soil hydrological characterization in rainfall-induced shallow landslides prone areas," *Bulletin of Engineering Geology and the Environment*, vol. 83, no. 5, Apr. 2024, Art. no. 167, https://doi.org/10.1007/s10064-024-03627-8.

[5] R. Abid, N. Kamoun, F. Jamoussi, and H. El Feki, "Fabrication and properties of compressed earth brick from local Tunisian raw materials," *Boletín de la Sociedad Española de Cerámica y Vidrio*, vol. 61, no. 5, pp. 397–407, Sep. 2022, https://doi.org/10.1016/j.bsecv.2021.02.001.

[6] S. N. Malkanthi, A. A. D. A. J. Perera, G. H. Galabada, and P. D. Dharmaratne, "Enhancement of the Properties of Compressed Stabilized Earth Blocks through the Replacement of Clay and Silt with Fly Ash," *Engineering, Technology & Applied Science Research*, vol. 11, no. 6, pp. 7927–7931, Dec. 2021, https://doi.org/10.48084/etasr.4580.

[7] S. N. Malkanthi and A. A. D. A. J. Perera, "Particle Packing Application for Improvement in the Properties of Compressed Stabilized Earth Blocks with Reduced Clay and Silt," *Engineering, Technology & Applied Science Research*, vol. 9, no. 4, pp. 4538–4542, Aug. 2019, https://doi.org/10.48084/etasr.3002.

[8] F. Champiré, A. Fabbri, J.-C. Morel, H. Wong, and F. McGregor, "Impact of relative humidity on the mechanical behavior of compacted earth as a building material," *Construction and Building Materials*, vol. 110, pp. 70–78, May 2016, https://doi.org/10.1016/j.conbuildmat.2016.01.027.

[9] S. S. Bibang Bi Obam Assoumou, L. Zhu, and C. Francis Deng, "A Conceptual Framework for Achieving Sustainable Building Through Compressed Earth Block: a Case of Ouagadougou, Burkina Faso," *Circular Economy and Sustainability*, vol. 3, no. 2, pp. 1029–1043, Jun. 2023, https://doi.org/10.1007/s43615-022-00213-6.

[10] L. Zhang, L. Yang, B. P. Jelle, Y. Wang, and A. Gustavsen, "Hygrothermal properties of compressed earthen bricks," *Construction and Building Materials*, vol. 162, pp. 576–583, Feb. 2018, https://doi.org/10.1016/j.conbuildmat.2017.11.163.

[11] L. Laou, J. E. Aubert, S. Yotte, P. Maillard, and L. Ulmet, "Hygroscopic and mechanical behaviour of earth bricks," *Materials and Structures*, vol. 54, no. 3, May 2021, Art. no. 116, https://doi.org/10.1617/s11527-021-01701-1.

[12] F. Abdulsamad, T. Chitimbo, A. Revil, N. Prime, and O. Plé, "Imaging the water content of rammed earth materials with induced polarization," *Engineering Geology*, vol. 322, Sep. 2023, Art. no. 107182, https://doi.org/10.1016/j.enggeo.2023.107182.

[13] D. Allinson and M. Hall, "Hygrothermal analysis of a stabilised rammed earth test building in the UK," *Energy and Buildings*, vol. 42, no. 6, pp. 845–852, Jun. 2010, https://doi.org/10.1016/j.enbuild.2009.12.005.

[14] P. Maillard and J. E. Aubert, "Effects of the anisotropy of extruded earth bricks on their hygrothermal properties," *Construction and Building Materials*, vol. 63, pp. 56–61, Jul. 2014, https://doi.org/10.1016/j.conbuildmat.2014.04.001.

[15] A. W. Bruno, B. Scott, Y. D'Offay-Mancienne, and C. Perlot, "Recyclability, durability and water vapour adsorption of unstabilised and stabilised compressed earth bricks," *Materials and Structures*, vol. 53, no. 6, Dec. 2020, Art. no. 149, https://doi.org/10.1617/s11527-020-01585-7.

[16] P. Brunet, R. Clément, and C. Bouvier, "Monitoring soil water content and deficit using Electrical Resistivity Tomography (ERT) – A case study in the Cevennes area, France," *Journal of Hydrology*, vol. 380, no. 1–2, pp. 146–153, Jan. 2010, https://doi.org/10.1016/j.jhydrol.2009.10.032.

[17] M. H. Loke, J. E. Chambers, D. F. Rucker, O. Kuras, and P. B. Wilkinson, "Recent developments in the direct-current geoelectrical imaging method," *Journal of Applied Geophysics*, vol. 95, pp. 135–156, Aug. 2013, https://doi.org/10.1016/j.jappgeo.2013.02.017.

[18] U. Singh and P. K. Sharma, "Study on geometric factor and sensitivity of subsurface for different electrical resistivity Tomography Arrays," *Arabian Journal of Geosciences*, vol. 15, no. 7, Mar. 2022, Art. no. 560, https://doi.org/10.1007/s12517-022-09844-3.

[19] S. Zhao, Z. Wei, Z. Xing, Y. Wu, S. Guo, and B. Liu, "Visualization investigation of defects in structural steel materials with electrical resistance tomography," *Construction and Building Materials*, vol. 356, Nov. 2022, Art. no. 129274, https://doi.org/10.1016/j.conbuildmat.2022.129274.

[20] A. Akhnoukh, "Overview of Concrete Durability Evaluation Using Electrical Resistivity," in *Collaboration and Integration in Construction, Engineering, Management and Technology*, Cham, 2021, pp. 9–14, https://doi.org/10.1007/978-3-030-48465-1_2.

[21] K. Karhunen, A. Seppänen, A. Lehikoinen, P. J. M. Monteiro, and J. P. Kaipio, "Electrical Resistance Tomography imaging of concrete," *Cement and Concrete Research*, vol. 40, no. 1, pp. 137–145, Jan. 2010, https://doi.org/10.1016/j.cemconres.2009.08.023.

[22] J. F. Lataste, C. Sirieix, D. Breysse, and M. Frappa, "Electrical resistivity measurement applied to cracking assessment on reinforced concrete structures in civil engineering," *NDT & E International*, vol. 36, no. 6, pp. 383–394, Sep. 2003, https://doi.org/10.1016/S0963-8695(03)00013-6.

[23] T. A. Nguyen, "Approches expérimentales et numériques pour l'étude des transferts hygroscopiques dans le bois," PhD dissertation, Université de Limoges, Limoges, France, 2014.

[24] W. Hafsa *et al.*, "Assessment of moisture content profile in Douglas-fir wood using electrical resistivity-based tomography," *Construction and Building Materials*, vol. 366, Feb. 2023, Art. no. 130193, https://doi.org/10.1016/j.conbuildmat.2022.130193.

[25] T. A. Nguyen, "Numeric Validation of the Inversion Model of Electrical Resistivity Imaging Method using the Levenberg-Marquardt Algorithm," *Engineering, Technology & Applied Science Research*, vol. 14, no. 1, pp. 12806–12811, Feb. 2024, https://doi.org/10.48084/etasr.6705.

[26] L. Laou, "Evaluation du comportement mécanique sous sollicitations thermohydriques d'un mur multimatériaux (bois, terre crue, liants minéraux) lors de sa construction et de son utilisation," PhD dissertation, Université de Limoges, Limoges, France, 2017.

[27] P. Rochowski and G. Pontrelli, "Mass diffusion in multi-layer systems: an electrical analogue modelling approach," *Computers in Biology and Medicine*, vol. 148, Sep. 2022, Art. no. 105774, https://doi.org/10.1016/j.compbiomed.2022.105774.

[28] A. Combescure, A. Hoffmann, and P. Pasquet, "The CASTEM Finite Element System," in *Finite Element Systems: A Handbook*, C. A. Brebbia, Ed. Berlin, Heidelberg: Springer, 1982, pp. 115–125.